In conclusion, it is shown (1) that the yield of neutral mesons by protons on protons at 440 Mev can be approximately obtained from the result at 340 Mev by a consideration of the energy dependence of meson production, and (2) that there is some evidence for the breakdown of the approximate selection rule which forbids the emission of s state mesons with final s state nucleons.

It is a pleasure to thank Professor E. M. McMillan for his continued interest in this experiment. I am grateful to Drs. J. Lepore, M. Ruderman, and P. Wolff for discussions of the theoretical aspects of the work. I also wish to express appreciation to Mr. J. Garrison for the loan of his liquid hydrogen target, and to the accelerator technical group under the direction of Mr. W. Stockton and Mr. D. O'Connell for their assistance in the construction of the Čerenkov counter. Thanks are also due to the cyclotron operating crew under Mr. J. Vale for their cooperation in making the bombardments.

PHYSICAL REVIEW VOLUME 92, NUMBER 3 NOVEMBER 1, 1953

Studies of X-Rays from Mu-Mesonic Atoms*

VAL L. FITCH AND JAMES RAINWATER
Department of Physics, Columbia University, New York, New York
(Received July 23, 1953)

A new technique of x-ray spectroscopy of μ-mesonic atoms has been developed. The x-rays are produced when a μ^-meson undergoes transitions between Bohr orbits about nuclei of various Z. The mesons are produced by the Columbia University 164-in. Nevis cyclotron. The x-rays are detected, and their energies are measured to better than 1 percent accuracy (for $Z \geq 22$) using a NaI crystal scintillation spectrometer. The $2p \rightarrow 1s$ transition energies were measured to be 0.35, 0.41, 0.955, 1.55, 1.60, 3.50, 5.80, 6.02, and 6.02 Mev for $Z=13$, 14, 22, 29, 30, 51, 80, 82, and 83. Special attention was paid to the Pb spectrum, and it is believed that an 0.2-Mev fine structure splitting has been observed. This is the expected splitting if the μ^- meson is a spin $\frac{1}{2}$ Dirac "heavy electron" of 210 electron masses, having the expected Dirac magnetic moment and having no strong nonelectromagnetic interaction with nuclear matter.

Since the μ^-meson Bohr orbits are 210 times closer to the nucleus than the equivalent electron orbits, the x-ray energies are quite sensitive to nuclear size for medium and large Z. In the case of Pb, a 1 percent change in nuclear radius gives a 1 percent change in the calculated x-ray energy. Assuming constant proton density inside a spherical nucleus of radius $R_0=r_0A^{\frac{1}{3}}$ and the above properties for the μ meson, we obtain $r_0=1.17$, 1.21, 1.22, and 1.17×10^{-13} cm for $Z=22$, 29, 51, and 82. The significance of these results in relation to other nuclear size measurements is discussed.

INTRODUCTION

WHEN a μ^- meson is slowed to rest in condensed matter through loss of its kinetic energy to electrons, it is captured in Bohr type orbits about a nucleus. Then, by a series of radiative and nonradiative (Auger) transitions, the meson proceeds to its K shell in an elapsed time of roughly 10^{-13} to 10^{-14} sec.[1] Thereafter, two competing mechanisms, natural beta decay and nuclear capture, account for the disappearance of the meson from the K shell. The characteristic decay time has been measured to be 2.1 μ sec. The mean time for nuclear capture has been investigated over a wide range of atomic numbers and has been found[2] to vary as Z^{-4} for low Z materials and saturate near 7×10^{-8} sec for $Z=82$. This is a manifestation of the extremely weak interaction (nonelectromagnetic) of μ mesons with nuclear matter. In comparison, the π^- meson will seldom reach the K shell except in the case of nuclei with low atomic number. Experimental studies of π-mesonic x-rays in light elements have been made[3] for low Z elements to investigate this strong absorption. Previously reported results[4] for μ^- mesons have been of a more qualitative nature than the present work and will not be discussed in detail since they are in rough agreement with the present more definite determinations of the transition energies.

When a μ^- meson is "stopped" in a target material and is captured in a Bohr orbit about a particular nucleus, the initial states are characterized by large quantum numbers n and l in view of the large statistical weight associated with these states. The decrease in n soon reaches the point where $n=l+1$, and subsequent transitions have $\Delta n=\Delta l=-1$. Thus the lower states in the cascade usually possess the largest l value consistent with the given total quantum number n (circular orbits).

* This research was supported by the joint program of the U. S. Office of Naval Research and the U. S. Atomic Energy Commission.

[1] E. Fermi and E. Teller, Phys. Rev. **72**, 399 (1947); see also R. E. Marshak, *Meson Physics* (McGraw-Hill Book Company, Inc., New York, 1952), Chaps. 5 and 6 for a general discussion of matters related to the present papers, and for further references.

[2] Keuffel, Harrison, Godfrey, and Reynolds, Phys. Rev. **87**, 942 (1952); see also J. M. Kennedy, Phys. Rev. **87**, 953 (1952).

[3] Camac, McGuire, Platt, and Schulte, Phys. Rev. **88**, 134 (1952).

[4] W. Y. Chang, Revs. Modern Phys. **21**, 166 (1949); E. P. Hinks, Phys. Rev. **81**, 313 (1951); G. G. Harris and T. J. B. Shanley, Phys. Rev. **89**, 983 (1953); F. D. S. Butement, Phil. Mag. **44**, 208 (1953); see G. R. Burbidge and A. H. de Borde, Phys. Rev. **89**, 189 (1953) for other references.

It has been shown[5] that the transitions involving states of high quantum number will be primarily nonradiative (Auger processes), while these in the region of low quantum number will be radiative. These x-rays have a small natural line width compared to the transitional energies between the lowest states. For example, in the case of lead the transition rate $2p\rightarrow 1s$ is approximately 10^{18} sec^{-1}, while the capture rate is approximately 10^{7} sec^{-1}. The resulting natural line width is approximately 1 kev for a total x-ray energy of 6 Mev.

Considering the nucleus as a point charge, the radius of a Bohr orbit is $2.82\times10^{-13}\ (m_e137^2/\mu Z)n^2$ cm, where m_e and μ represent the electron and μ^--meson masses. Thus the μ-mesonic orbit will be smaller than the corresponding electron orbit by the mass factor 210. In the case of lead this gives $r=3.07\times10^{-13}$ cm for $n=1$, which is well inside the nucleus, and $r=1.23\times10^{-12}$ cm for $n=2$, which is just outside the nuclear surface. Again in the case of Pb, the predicted $2p_{\frac{3}{2}}\rightarrow 1s$ transition energy for a point nucleus is 16.41 Mev, whereas we have measured the energy of this transition as 6.02 Mev. Thus the finite nuclear size results in almost a factor of three decrease in the transition energy. Assuming a nuclear model of constant density inside a sphere of radius R_0, with a sharp edge and zero density outside, we find that a 1 percent change in R_0 gives a 1 percent calculated change in the transition energy. Since the x-ray energy is measured to better than 1 percent accuracy, a corresponding accuracy is obtained for the best fitting value of R_0. This great sensitivity of the μ^- meson as a "probe" of the nucleus was first pointed out by Wheeler[5] and served as a stimulus for the research reported in this paper. This sensitivity to nuclear size decreases rapidly with decreasing Z and amounts to only a 2 percent total effect for aluminum. The transition energy is mainly sensitive to the meson mass rather than nuclear size for low Z, and mainly sensitive to nuclear size for high Z materials. By exploiting this fact we have obtained an independent evaluation of the μ-meson mass in agreement with the results of other techniques.

The fine structure splitting of the $2p$ level depends on the spin and magnetic moment of the μ meson which is usually assumed to be a Dirac particle of spin $\frac{1}{2}$. Thus the anomalous g factor of 2 is expected. Other spin $\frac{1}{2}$ particles believed to obey the Dirac theory include the electron, proton, neutron, and neutrino. The electron moment in the hydrogen atom is now known to be slightly different from one electron magneton, and this has recently been explained in terms of higher-order effects in quantum electrodynamics. The neutron and proton moments deviate considerably from the expected Dirac values of 0 and 1 nuclear magnetons, presumably because of their strong coupling to meson fields. The μ meson, unlike the nucleons, has no known strong (non-electromagnetic) coupling to other particles, and it is reasonable to expect, therefore, that its magnetic moment would be close to one μ-mesonic magneton if it is a spin $\frac{1}{2}$ Dirac type particle. (The $\pi^-\rightarrow\mu^-+\nu$ and $\mu^-\rightarrow e^-+2\nu$ processes and the nature of the stars produced following nuclear capture seem to require that the μ meson have Fermi-Dirac statistics, and thus odd half-integral spin.) Results of the investigation of cosmic-ray bursts seem to rule out spin $\frac{3}{2}$ or higher.

For spin $\frac{1}{2}$, the $2p$ level will split into $2p_{\frac{3}{2}}$ and $2p_{\frac{1}{2}}$ with relative statistical weighting factors of 2 and 1. (This weighting is found theoretically to apply even for the situation where the $2p$ level is reached by successive transitions having $\Delta n=\Delta l=-1$.) In the case of a point Pb nucleus, the expected fine structure splitting is 0.55 Mev. This is reduced to about 0.2 Mev for the actual size, and we believe that we have probably observed this fine structure splitting in the Pb spectrum. If the μ meson has spin 0, there would be no fine structure splitting. If its spin is 1 or more, there will be three lines in the fine structure. Thus a study of the fine structure can determine both the spin and magnetic moment of the μ meson.

This paper reports experimental studies of the x-rays from the $2p\rightarrow 1s$ transition in μ-mesonic atoms for $Z=13$, 14, 22, 29, 30, 51, 80, 82, and 83. The Columbia University Nevis Cyclotron produces an external meson flux which is collimated in the main shielding wall to produce meson beams of relatively well-defined momenta. The beams consist of both π and μ mesons, the mu's originating from decay of pi's close to the cyclotron target. The μ mesons with the same momenta as the π mesons have a greater range, thus the π mesons can be removed from the beam by using absorbers. The x-rays associated with the μ mesons stopping in various materials were studied using a NaI crystal spectrometer with an accuracy of about 1 percent or better in the energy determination, depending on the Z of the target material.

THEORY

Wheeler[5] has calculated the $1s$, $2p_{\frac{1}{2}}$, $2p_{\frac{3}{2}}$, and $2s_{\frac{1}{2}}$ levels for a μ^- meson of $200m_e$ in atoms of various Z. Since the results quoted were not found to be sufficiently accurate for a precise comparison with our experiments, we have recalculated these levels using more exact methods using $\mu=210m_e$ and a model of the nucleus having constant charge density to $R_0=1.30A^{\frac{1}{3}}\times10^{-13}$ cm, with zero density for $r>R_0$. The μ meson was assumed to obey the Dirac equation and only the electrostatic potential was considered. In this case the Dirac equation becomes[6]

$$[E-V+c\boldsymbol{\alpha}\cdot\mathbf{p}+\beta\mu c^2]\psi=0, \qquad (1)$$

[5] J. A. Wheeler, Revs. Modern Phys. **21**, 133 (1949); R. E. Marshak, reference 1, Chap. 5. See also G. R. Burbidge and A. H. de Borde, Phys. Rev. **89**, 189 (1953).

[6] See L. I. Schiff, *Quantum Mechanics* (McGraw-Hill Book Company, Inc., New York, 1949), Chap. 12 for derivations of the following equations, or of approximations to them. The notation follows that of Schiff for the most part.

where $E=\mu c^2+E'=$ total meson energy, and $E'=$ binding energy, V is the potential energy, and $\mathbf{p}$ is the meson momentum. $\boldsymbol{\alpha}$ and β are 4×4 Dirac operators. $\psi=\begin{pmatrix}\varphi_a\\ \varphi_b\end{pmatrix}$ is the 4-component wave function, where φ_a and φ_b, representing the (1, 2) and the (3, 4) terms of ψ respectively, are two-component functions. This is easily transformed to the form

$$\{(E-V)^2-c^2p^2-\mu^2c^4\}\psi-\left\{i\hbar c\left(\frac{1}{r}\frac{\partial V}{\partial r}\right)(\boldsymbol{\alpha}\cdot\mathbf{r})\right\}\psi=0, \quad (2)$$

where the first bracket corresponds to the Klein-Gordon equation appropriate for a spin zero particle, and the last term is the characteristic Dirac term. Expressed in terms of φ_a and φ_b, Eq. (2) becomes

$$\{(E-V)^2-c^2p^2-\mu^2c^4\}\varphi_a-\left\{i\hbar c\left(\frac{1}{r}\frac{\partial V}{\partial r}\right)(\boldsymbol{\sigma}\cdot\mathbf{r})\right\}\varphi_b=0, \quad (3a)$$

$$\{(E-V)^2-c^2p^2-\mu^2c^4\}\varphi_b-\left\{i\hbar c\left(\frac{1}{r}\frac{\partial V}{\partial r}\right)(\boldsymbol{\sigma}\cdot\mathbf{r})\right\}\varphi_a=0, \quad (3b)$$

where $\boldsymbol{\sigma}$ is the usual 2×2 Pauli spin operator ($\mathbf{S}=\hbar\boldsymbol{\sigma}/2$ = meson spin operator). Similar expansion of Eq. (1) gives two coupled equations for φ_a and φ_b in a form that shows that φ_b is the "larger" component for $E>0$ and yields the relation

$$\varphi_a=-c[E'+2\mu c^2-V]^{-1}(\boldsymbol{\sigma}\cdot\mathbf{p})\varphi_b. \quad (4)$$

On insertion of Eq. (4) in (3b), using $(\boldsymbol{\sigma}\cdot\mathbf{r})(\boldsymbol{\sigma}\cdot\mathbf{p})=\mathbf{r}\cdot\mathbf{p}+i\boldsymbol{\sigma}\cdot\mathbf{L}$, where $\mathbf{L}=\mathbf{r}\times\mathbf{p}=$orbital angular momentum, this gives the exact relation

$$\{(E-V)^2-c^2p^2-\mu^2c^4\}\varphi_b+\frac{\hbar}{2}\left[1+\frac{(E'-V)}{2\mu c^2}\right]^{-1}\frac{\partial V}{\partial r}\left[\frac{\partial}{\hbar\partial r}-(\boldsymbol{\sigma}\cdot\mathbf{L})\right]\varphi_b=0. \quad (5)$$

The first bracket again contains the Klein-Gordon term and the last contains the characteristic Dirac terms. In the last bracket, the second term gives the usual spin-orbit interaction. Since $\boldsymbol{\sigma}\cdot\mathbf{L}$ and L^2 are not constants of the motion, it is perferable to use the variable $\hbar k=\beta(\boldsymbol{\sigma}'\cdot\mathbf{L}+\hbar)$ which is a constant of the motion. Here $|k|=(j+\frac{1}{2})$, and $k=-1$, $+1$, and -2 for the $1s_{\frac{1}{2}}$, $2p_{\frac{1}{2}}$, and $2p_{\frac{3}{2}}$ states, respectively. The Dirac equation reduces to a purely radial equation for a two component wave function with components $[F(r)/r]$ and $[G(r)/r]$ respectively, where G is the "large" component function in the coupled equations:

$$(E'+2\mu c^2-V)F-\hbar c\left(\frac{d}{dr}+\frac{k}{r}\right)G=0, \quad (6a)$$

$$(E'-V)G+\hbar c\left(\frac{d}{dr}-\frac{k}{r}\right)F=0. \quad (6b)$$

Solving Eq. (6a) for F and substituting in (6b) gives

$$\left\{(2\mu c^2+E'-V)^2-\mu^2c^4+\hbar^2c^2\left[\frac{d^2}{dr^2}-\frac{k(k+1)}{r^2}\right]\right\}G+\left\{\frac{\hbar^2}{2}\left[1+\frac{(E'-V)}{2\mu c^2}\right]^{-1}\frac{dV}{dr}\left[\frac{d}{dr}+\frac{k}{r}\right]\right\}G=0, \quad (7)$$

which is similar to Eq. (5). Since the second bracket Dirac terms are small compared to the first bracket main Klein-Gordon term, there is very little error made by replacing $[1+(E'-V)/2\mu c^2]^{-1}$ in the second bracket by unity. This is usually done.

In the case of a point nucleus Eqs. (6a, b) may be solved exactly to give

$$E'=\mu c^2\left\{\left[1+\frac{(Z/137)^2}{\{n-|k|+[k^2-(Z/137)^2]^{\frac{1}{2}}\}^2}\right]^{-\frac{1}{2}}-1\right\}, \quad (8)$$

where the fine structure constant is taken approximately as 1/137.

The energies given by Eq. (8) are listed in Table I for selected values of Z along with the modified values using $R_0=1.3A^{\frac{1}{3}}\times10^{-13}$ cm and a nucleus of uniform charge distribution. Several methods of varying precision were used to obtain the values listed for finite nuclear radius. Particular attention was paid to the case of Pb($Z=82$) since the various corrections to approximate calculations are most serious for high Z, and since Pb is a particularly interesting material to

TABLE I. Calculated energies of μ-meson orbits for $\mu=210m_e$. All energies are in Mev.

	Dirac energies $R_0=0$			Dirac energies $R_0=1.3A^{\frac{1}{3}}\times10^{-13}$ cm			Klein-Gordon energies $R_0=1.3A^{\frac{1}{3}}\times10^{-13}$ cm	
Z	$E(1s)$	$2p_{\frac{1}{2}}\to1s$	$2p_{\frac{3}{2}}\to1s$	$E(1s)$	$2p_{\frac{1}{2}}\to1s$	$2p_{\frac{3}{2}}\to1s$	$E(1s)$	$2p\to1s$
13	0.4849	0.3631	0.3628					
14	0.5614	0.4213	0.4209					
22	1.3917	1.0455	1.0432	1.282	0.935	0.933		
29	2.4300	1.8277	1.8208	2.12	1.52	1.51		
30	2.6026	1.9579	1.9500					
51	7.7071	5.8332	5.7627	5.22	3.41	3.37		
80	20.181	15.508	15.011					
82	21.328	16.414	15.857	10.11	5.48	5.30	10.24	5.52
83	21.919	16.880	16.291					

TABLE II. Comparison of the calculated μ-meson orbit energies for Pb using the various computational methods discussed in the text.

	Dirac energies	Klein-Gordon energies	Klein-Gordon correction terms $\frac{1}{r}\left(\frac{dV}{dr}\right)\mathbf{L}\cdot\mathbf{S}$	Klein-Gordon correction terms $\frac{dv}{dr}\frac{d\psi}{dr}$	Klein-Gordon energies plus correction terms
$E(1s)$	-10.11	-10.24		$+0.157$	-10.08
$E(2p_{\frac{1}{2}})$	-4.807	-4.72	-0.125	$+0.032$	-4.81
$E(2p_{\frac{3}{2}})$	-4.63	-4.72	$+0.062$	$+0.032$	-4.63

use to investigate the fine structure splitting. We include a discussion of the more approximate methods to illustrate the order of magnitude of the different terms and the errors introduced by various approximate methods. The first method used the Klein-Gordon

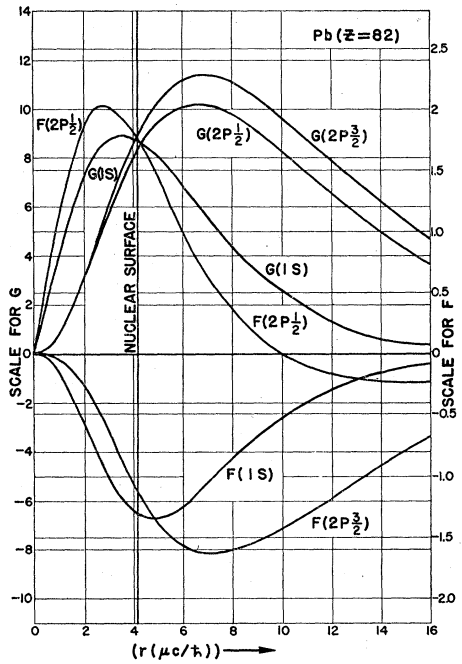

FIG. 1. The $1s$, $2p_{\frac{1}{2}}$, and $2p_{\frac{3}{2}}$ unnormalized meson radial wave functions G and F [of Eq. (6a, b)] in the field of a Pb nucleus. A uniform nuclear model is used with $r_0=1.3\times10^{-13}$ cm. Radii are expressed in units of $h/\mu c=1.84\times10^{-13}$ cm, with the position of the nuclear surface (4.18 units) indicated.

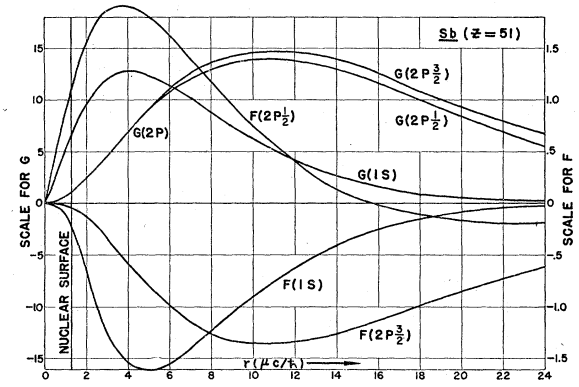

FIG. 2. Curves similar to those of Fig. 1, but for Sb($Z=51$). The nuclear surface is at 2.62 units of radius. *Note added in proof:* The position of the nuclear surface is shown incorrectly in the figure.

equation and the $V(r)$ for finite nuclear size. A point by point method of numerical integration was employed, trying various grid lengths, starting at $r=0$ and continuing until it was clear that E' had been chosen too large or too small. This method was poor for the L shell due to the $2/r^2$ angular momentum term, and a (semiconvergent) series method was tried and found to be much easier to use. In the case of $r<R_0$ a series in positive powers of r was used. For $r>R_0$ a solution of the form $e^{-br}r^m\sum a_n r^{-n}$ was used. The values of (G'/G) for the two functions at $r=R_0$ were compared as a function of E', with the correct value usually determined by interpolation after the first two trials. The $(dV/dr)(dG/dr)$ and the $(k/r)(dV/dr)G$ terms in Eq. (7) were then treated as perturbations and evaluated by first-order perturbation theory with the results shown in Table II. Similarly, the effect of changing the value of the nuclear radius R_0 was evaluated in the Klein-Gordon term by treating the *difference* in V for the two choices of R_0 as a perturbation. It was found that an attempt to calculate the effect of finite nuclear radius by using $R_0=0$ functions to calculate the entire effect as a first-order perturbation gave quite poor results. However, the result of a change of ±10 percent in R_0 about the chosen radius is given with good accuracy.

It was later found to be feasible to carry out the (semiconvergent) series expansions of the inside and outside functions, using the complete coupled equations (6a, b) directly, and this has been carried through for a number of cases with results in close agreement with the previous method. For a given l and j, the G function starts as r^{l+1} and the F function as r^l when $j=l-\frac{1}{2}$, and as r^{l+2} when $j=l+\frac{1}{2}$. A plot of these unnormalized functions for Pb and Sb ($Z=82$ and 51) are shown in Figs. 1 and 2, where the F and G functions are shown with the proper relative amplitudes indicated by the two ordinate scales.

Additional effects of interest include (a) the effect of the polarization of the nucleus by the μ meson, (b) the hyperfine splitting due to the nuclear magnetic moment for odd-A nuclei (Pb has mainly spin-zero isotopes), (c) the effect of a nuclear electrical quadrupole moment, (d) the effect of nonuniform charge distribution as a function of r within the nucleus, including the effect of an expected gradual dropping off of the nuclear charge density beyond the nuclear "surface," (e) the effect of other forces not considered, or of a different spin for the μ meson.

Cooper and Henley[7] have studied some of these effects. They estimate that nuclear polarizability may effect the Pb transition energies by about 0.06 Mev or less (a 1 percent effect or less) and set 0.15 Mev as an upper limit for this effect. Wheeler[4] has calculated the hyperfine splitting for Al($Z=13$) as 9.7 ev. For higher Z the splitting should vary more slowly than Z^3, so the splitting would probably be less than 1 kev in all cases.

The effect of the quadrupole splitting has been investigated by Wheeler.[8] It should be negligible for the materials reported in this paper. The possibility of spin $\frac{1}{2}$ will affect the number of fine structure lines and

[7] L. Cooper and E. Henley (following article), Phys. Rev. **92**, 801 (1953).

[8] J. A. Wheeler (Paper III of this series), Phys. Rev. **92**, 812 (1953).

would be observed experimentally. The existence of any other important attractive interaction between the μ meson and nuclei seems very unlikely but cannot be completely excluded. It would shift the energies in a manner similar to that of a decrease in nuclear radius.

EXPERIMENTAL METHOD

The two main facilities required for this experiment are (1) a source of reasonably monoenergetic μ^- mesons which can be made to stop in a relatively thin target material of selected atomic number under conditions such that the background radiation effects are not too severe, and (2) a photon detector of high sensitivity and good energy selection for the region of 50 kev to 10 Mev.

The μ^- mesons were obtained as follows. Referring to the floor plan, Fig. 3, the 385-Mev protons rotating clockwise inside the cyclotron chamber strike a thin Be target and produce various reaction products including fast neutrons, π^+, π^-, and π^0 mesons, which are emitted in all directions. Near the target the π^0 mesons decay to photons and eventually some electron-positron pairs are formed. These contribute some

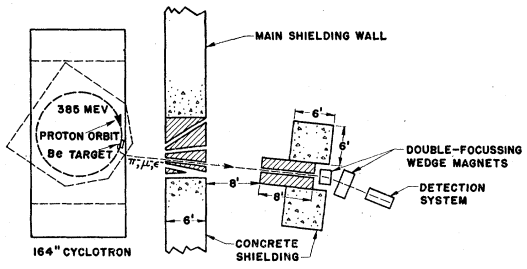

FIG. 3. Floor plan showing location of cyclotron shielding, focusing magnets, and detection system. A typical meson path is shown.

electrons to the final beam. The π^- mesons of approximately 100-Mev kinetic energy have a mean path of approximately 10 meters for $\pi^-\rightarrow\mu^-+\nu$ decay and a certain fraction decay near the target, where the π^- density is highest. The fringing magnetic field of the cyclotron provides a horizontal focusing action for negative particles of any definite energy group emitted in the horizontal plane at angles inward from the forward proton direction. Ports through the shielding wall then serve to select definite momentum beams of negative particles. A beam analysis indicates that approximately 10 percent of the beam particles are μ^- mesons of the same momentum as the π^- mesons. Most of the μ^- mesons originating from decay of the pi's in the beam are projected out of the beam and lost. A typical useful path is indicated in Fig. 3.

The general level of background radiation in the region just outside the shielding was found to be too large for successful performance of this experiment, mainly as a result of the secondary effects of fast neutrons. The method finally employed to reduce background in the photon detector to a reasonable level

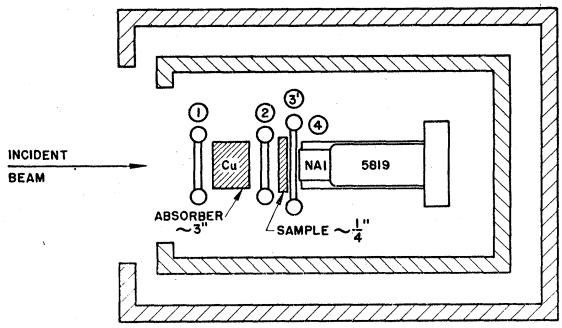

FIG. 4. Diagram of detection system. Stilbene scintillation counters 1, 2, and 3' select particles stopping in the sample material. NaI scintillation counter 4 serves as the photon detector. The copper absorber between counters 1 and 2 removes the π mesons from the beam. Magnetic shielding is provided by a double walled box of $\frac{1}{2}$-in. iron plate.

is shown in Fig. 3. A secondary barricade of concrete blocks was used starting 8 feet from the main shielding wall. The beam traversed a 6-in. diameter hole in an 8-ft long shielding block and was then double-focused using two magnets having triangular "wedge" pole faces. The magnets served to deflect the beam from the direct line of the collimator and to concentrate it at the detection system.

The detection system is illustrated in Fig. 4. Counters 1, 2, and 3 consist of stilbene scintillation crystals viewed by 1P21 phototubes. Counter 4 functions as the photon detector. It consists of a NaI(Tl) crystal viewed by a 5819 phototube. All pertinent counter dimensions are listed in Table III. For the purpose of shielding the phototubes from stray magnetic fields the whole detection system is surrounded by a double-walled steel box made of $\frac{1}{2}$-in. material except in the region where the meson beam enters. This assembly was then mounted on an adjustable rolling cart.

The beam was analyzed as follows. One inch of carbon

TABLE III. Approximate values of counting parameters.

1. (1, 2) rate, no absorber: 450/sec.
2. (1, 2) rate, full absorber: 50/sec.
3. Approximate beam composition:
   115-Mev $\pi^-\approx 90\%$
   130-Mev $\mu^-\approx 10\%$
   214-Mev $e^-< 3\%$
4. Detector dimensions:

Counter	Diameter, in.	Thickness, in.
1	2	$\frac{1}{8}$
2	2	$\frac{1}{8}$
3	3	$\frac{1}{4}$
4	$1\frac{1}{2}$	1

5. Approximate interval counting rate of the x-ray. Analyzer near the peak of the spectrum.

Element	Interval width	Interval counts/min
Pb (5 Mev)	100 kv	1
Cu (1.53 Mev)	50 kv	2
Al (0.35 Mev)	20 kv	6

was placed in the sample position directly in front of counter 3, and a count of 123′ (123′ denotes coincidence between counters 1 and 2 and anticoincidence with counter 3) was taken as a function of copper thickness yielding a differential range curve of the meson beam. The beam was monitored by a second counter telescope positioned in one of the other beams. A sample curve is shown in Fig. 5. Two groups of particles with the same momentum are present. If the short range group is identified as π mesons then from range consideration the particles in the second group must have a mass of approximately 210 electron masses, and these are identified as μ mesons. For a further check on this identification, the decay of the μ meson to an energetic electron was utilized. An organic crystal of 1 square inch replaced the NaI crystal as counter 4. A delayed coincidence between counters 3 and 4 was tabulated in 8

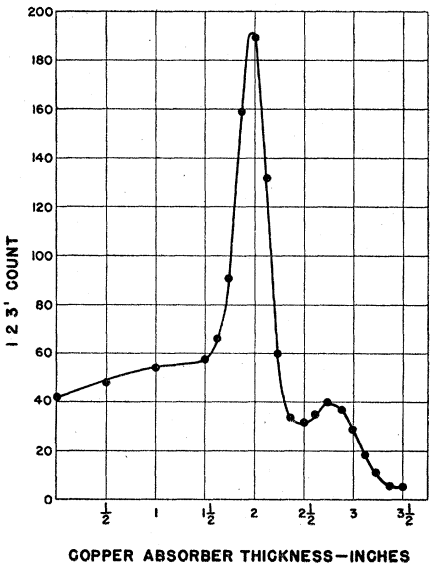

FIG. 5. Differential range curve of the meson beam. The peaks at 2 in. and $2\frac{3}{4}$ in. correspond to π and μ mesons respectively.

consecutive time intervals each approximately one microsecond in duration. The timing chain was triggered by 123′. Subtraction of the sum of the counts received in the final four channels from the sum of those in the initial four channels gives a measure of the short-lived activity associated with particles stopping in the carbon sample. This measurement was made as a function of copper absorber thickness between counters 1 and 2. The results are plotted in Fig. 6. It is observed that the delayed activity is a maximum for that thickness of copper which corresponds to the range of the second group of particles in Fig. 5. This delayed activity we associate with the decay of the μ^- mesons in the carbon. That the thickness of copper determined in this way was the optimum value was confirmed later by examining the μ-mesonic x-ray spectra as a function of copper thickness.

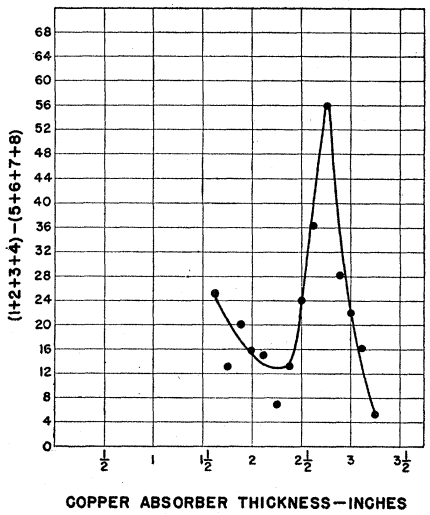

FIG. 6. Delayed activity [channels (1+2+3+4)−(5+6+7+8)] associated with particles stopping in carbon sample as a function of copper thickness between counters 1 and 2.

When the NaI detector pulses were also analyzed for pulse height to measure the photon energy, a fast 1, 2, 3′, 4 coincidence, using the collector anode of the 5819 tube, was used to trigger the pulse height analyzer which then measured the slower pulse from the 8th dynode of the 5819 tube. Provisions were also made to render the circuit insensitive for approximately 8 microseconds after each NaI pulse to assure complete recovery of the pulse level to the reference value. A thermostatic temperature control for the detector box was found to improve stability.

In addition to the NaI photon detector, the scintillation spectrometer consisted of a 10-channel differential pulse-hieght analyzer and associated amplifiers, scaling circuits, and registers. For the measurements reported here, the pulse-height analyzer was adjusted to separate the pulse spectrum into sixty intervals, which could be explored ten at a time. Thus, over a 6-Mev energy spectrum, the minimum channel width was 100 kev. All amplifier circuits were designed for optimum stability consistent with reasonable speed and insensitivity to extreme overload both in pulse rate and amplitude. The over-all spectrometer system was stable to better than $\frac{1}{2}$ percent over operating periods of three days.

Interpretation of the NaI pulse-height distribution is somewhat complicated by the fact that the primary processes by which the photon loses energy to the NaI crystal above 1 Mev are the Compton scattering and pair production. Figure 7 shows the probability per cm *vs* photon energy, of a primary interaction corresponding to photoelectric absorption, Compton scattering, or pair production. The photoelectric effect becomes negligible above approximately 1 Mev but is important at lower energies, particularly for the absorption of lower-energy Compton scattered photons.

The energy transfer in the Compton scattering of a photon of energy E_0 shows a continuous distribution from zero to about $(E_0-0.25)$ Mev (the energy transfer for backscattering). The distribution rises to a sharp peak at the high-energy end,[9] and this peak is evident when a thinner NaI crystal is used. However, the scattered photons here have approximately 0.25 Mev and are strongly absorbed in a thick detector. Thus the upper end of the Compton distribution is depleted and contributes somewhat to a full energy peak. This is again complicated, in principle, by the fact that the range of the knock-on electrons, for approximately 5-Mev photons, is not small compared to a radiation length in NaI and brehmsstrahlung processes should occur frequently. Fortunately this mainly involves the

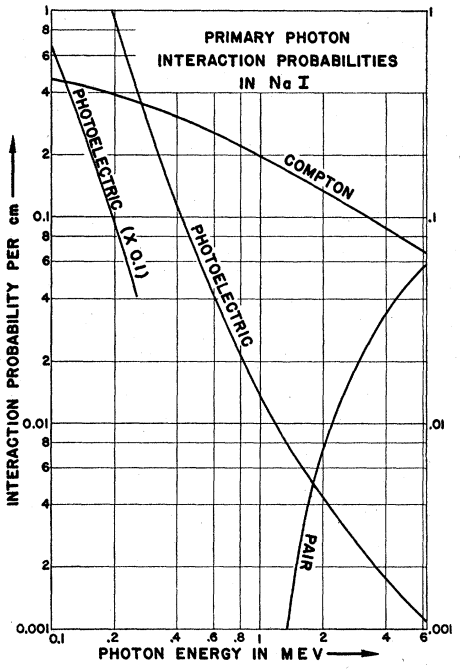

FIG. 7. The probabilities per cm of path in NaI of photoelectric absorption, Compton scattering, or pair production primary interactions as a function of photon energy.

emission of low-energy x-rays which are readily absorbed.

The pair production process becomes increasingly important as the energy is increased above approximately 2 Mev. However, the direct pair process gives a pulse 1.02 Mev lower than the full energy with two 0.511-Mev annihilation gamma rays emitted when the positron stops. Again, one or both of these secondary photons may be wholly or partially absorbed to contribute to a peak at $(E_0-0.51$ Mev), or at E_0.

The curves of Fig. 7 thus are useful in showing the efficiency of various primary processes as a function of primary photon energy, but they do not tell the full story because of the complications of secondary processes. The spectrum shape $f(E_0, E)$ obtained from a photon of energy E_0 is thus a complicated function of E_0 and E which, we believe, cannot readily (or reliably) be computed by multiple application of the laws for primary interactions. It is thus necessary to obtain $f(E_0, E)$ experimentally by using known energy calibration sources. This problem is separate from the calibration of the pulse height scale in energy units. We have detected no observable deviation from linearity in the calibration of pulse height *vs* energy based on the comparison of pulse-height distribution curves using photons of the following energies: annihilation photons (0.511 Mev); Cs^{137} photons (0.662 Mev), Na^{24} photons (1.38, 2.76 Mev), C^{12*} photons (4.43 Mev), and Co^{60} (1.17, 1.33 Mev) photons, for the full energy and the different reduced energy peaks.

The spectrometer energy calibration was performed occasionally during cyclotron runs by measuring the pulse spectrum of the gamma rays from Na^{24}. The extrapolation to higher energies was accomplished by the use of carefully calibrated attenuators in the amplifier circuits. Confidence in the method was established by comparing the measured energies of known gamma rays using the same attenuation settings. Possible rate dependence of the measured pulse amplitude was explored by subjecting the spectrometer to background radiation from natural sources which

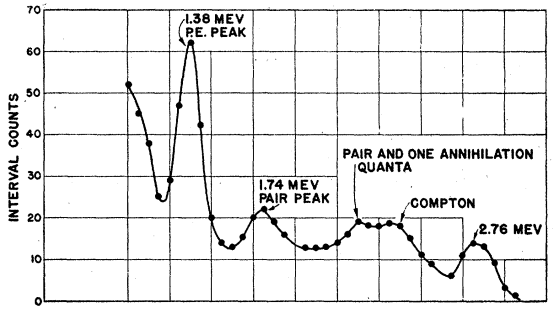

FIG. 8. Typical energy calibration curve using Na^{24}. The two γ rays at 2.76 and 1.38 Mev occur in equal number. The relative heights of the various peaks gives information about the relative efficiencies of the several interaction processes in NaI.

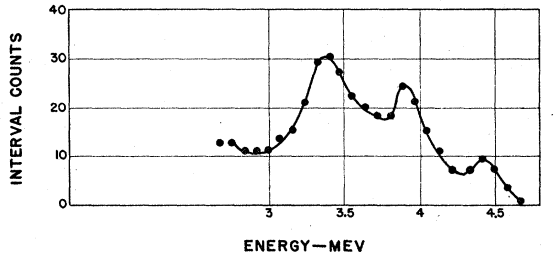

FIG. 9. Pulse-height distribution for the 4.43-Mev γ rays from C* produced in the reaction $\alpha+Be^9\rightarrow C^{12*}+n$, using Po as a source of α particles. The peaks show a Doppler broadening of $\sim$2 percent due to the motion of the C^{12*} nuclei.

[9] C. M. Davisson and R. D. Evans, Revs. Modern Phys. 24, 79, (1952). See Fig. 49 for several such plots. (The curves in Fig. 8 were calculated from Table XIV of this reference.)

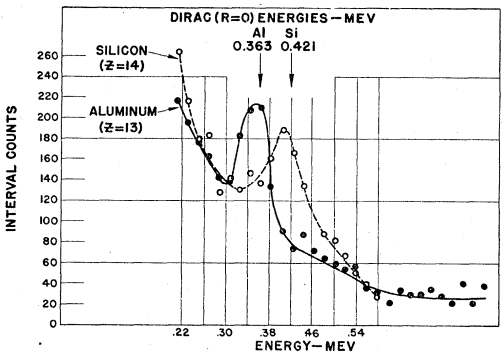

FIG. 10. Pulse-height distribution using Al and Si as the target materials ($Z=13$, 14). The peaks represent the full energies of the x-rays emitted in the $2p\rightarrow 1s$ transition. The expected energies for a point nucleus using $\mu=210m_e$ are included for reference. The shift in energy due to the finite extension of the nucleus is ~2 percent. In the case of Al in the region below 0.39 Mev the points are based on double the indicated number of counts. The interval width is approximately 50 kev.

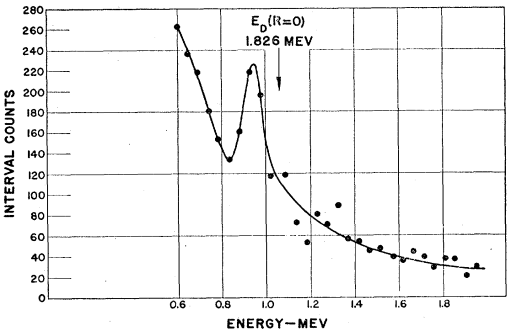

FIG. 11. Pulse-height distribution for Ti($Z=22$). The energy shift of 5 percent of the measured value due to finite nuclear extension is apparent. (In the figure 1.826 mev should read 1.045 mev.)

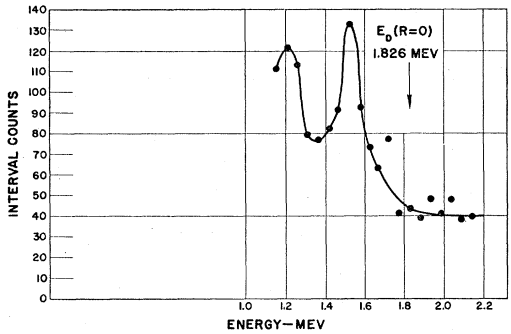

FIG. 12 Pulse-height distribution for Cu($Z=29$). Above 1.7 Mev the points are based on 0.6 the indicated number of counts. The energy shift due to finite nuclear extension is 18 percent of the measured value.

contributed a pulse rate that was considerably higher than the instantaneous rates encountered when using the cyclotron. No shift in pulse amplitude was observed until the rate was about four times the instantaneous rate experienced with the cyclotron. Also large variations in the cyclotron intensity did not cause noticeable shifts in the positions of the peaks.

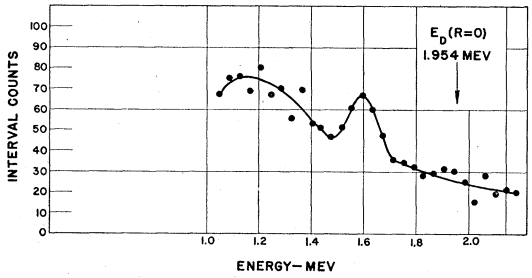

FIG. 13. Pulse-height distribution of Zn($Z=30$). In the region of the peak the points are based on 3 times the indicated number of counts. The energy shift due to finite nuclear extension is 22 percent of the measured value.

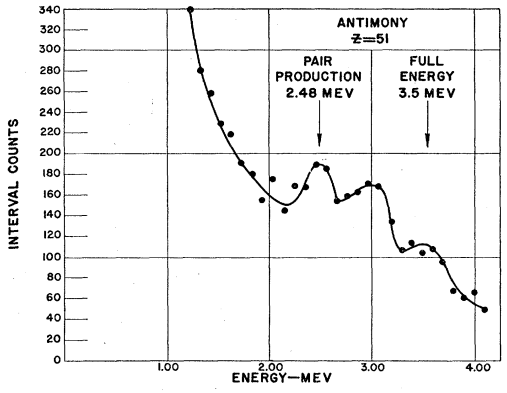

FIG. 14. Pulse-height distribution for Sb($Z=51$). The three peaks expected for a single photon of this energy are observed. The energy shift due to finite nuclear extension is 66 percent of the measured value.

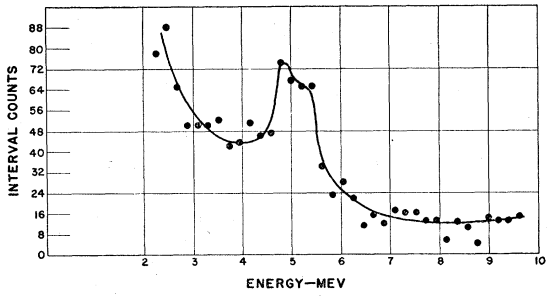

FIG. 15. Pulse-height distribution for Pb($Z=82$) taken with relatively coarse resolution (212 kev) and poor statistics over a wide energy range. The distinctive peak around 5 Mev defines the region of interest which was then investigated with higher resolution as is shown in the next figure.

Interpretation of the observed pulse height distribution curves is facilitated by examination of the Na^{24} and C^{12*} calibration curves of Figs. 8 and 9. In Fig. 9 the full energy peak of the 2.76-Mev photon is due mainly to the backward Compton scattering followed by the absorption of the secondary photon. The full energy peak for the 1.38-Mev photon is much larger. The 2.76-Mev photon also contributes peaks corresponding to pair production, and pair plus one annihilation photon. The effect of the Compton scattering, modified by some secondary absorption is also evident for the

2.76-Mev photon. It is important to remember that the 2.76- and 1.38-Mev photons are in cascade and are thus emitted in equal number. The relative peak heights thus give direct evidence concerning the relative efficiencies of various processes for these two energy photons.

Figure 9 shows the pulse spectrum resulting from the radiation from the Po-Be neutron source. The 4.43-Mev gamma rays result from a transition from the first excited level[10] of O^{12} to the ground state following the neutron-producing reaction. The source is uot monochromatic but shows a 2 percent Doppler broadening due to the momentum of the C^{12*} nucleus in the reaction. This Doppler broadening affects the shape of the pulse-height curve since the peaks would be expected to be significantly higher and narrower for a monochromatic source.

The coincidence resolution was somewhat better than 10^{-7} sec. This is sufficient to remove from the spectrum approximately half of the gamma rays originating from nuclear capture of the μ^- meson in the high-Z materials, and essentially all of them for lower-Z materials where nuclear absorption is slower.

EXPERIMENTAL RESULTS

The pulse-height distribution curves of Figs. 10 to 18 show the experimental results for studies of the x-rays resulting when μ^- mesons are stopped in Al, Si, Ti, Cu, Zn, Sb, Pb, Hg, and Bi ($Z=13$, 14, 22, 29, 30, 51, 82, 80, and 83). In the first few curves the predicted full energy position of the $2p\rightarrow 1s$ transition for a point nucleus is shown for reference (using $\mu=210m_e$). The x-ray energies vary from about 0.35 Mev for Al to 6.0 Mev for Pb and Bi. In the cases of Al, Si, Ti, Cu, and Zn, the main x-ray peak occurs at the full energy and general background and Compton scattering pulses contribute other pulse heights to the spectrum. For Sb the full energy occurs at about 3.5 Mev and three peaks, like those of Fig. 9, are obtained for E_0, $E_0-0.51$ Mev and $E_0-1.02$ Mev superimposed on a general background level.

Figure 15 shows the results for Pb over a region from about 2 Mev to 10 Mev using an interval width of about 210 kev. The x-ray peak stands out strongly near 5 Mev. The region from 4.2 to 6.0 Mev was then investigated using approximately 100-kv resolution width, with the typical results given in Fig. 16. This curve should be compared with Fig. 9 for interpretation. We have adopted, as most likely, the interpretation that the 5.0-Mev peak is the $2p_{\frac{3}{2}}\rightarrow 1s$ pair peak corresponding to 6.0 Mev for the x-ray energy. The $2p_{\frac{1}{2}}\rightarrow 1s$ peak should be 0.2 Mev lower in energy with half the intensity of the other. The peak near 5.3 Mev and the effects near 4.8 Mev and 5.6 Mev are not consistent with the pattern of Fig. 9 of three nearly symmetric peaks 0.5 Mev apart. In using Fig. 9 for reference, it should be noted that theoretical considerations, and the experimental results of other investigators (using similar sized NaI crystals), show that the pair peak should be relatively much larger compared to the intermediate and full energy peaks at 6 Mev than for 4.5-Mev photons.

Our tentative interpretation of Fig. 16 is thus that there are present $2p_{\frac{3}{2}}\rightarrow 1s$ and $2p_{\frac{1}{2}}\rightarrow 1s$ x-rays of 6.0 and 5.8 Mev respectively. The main peak at 5.0 Mev and the shoulder at 5.5 Mev followed by a sharp drop at

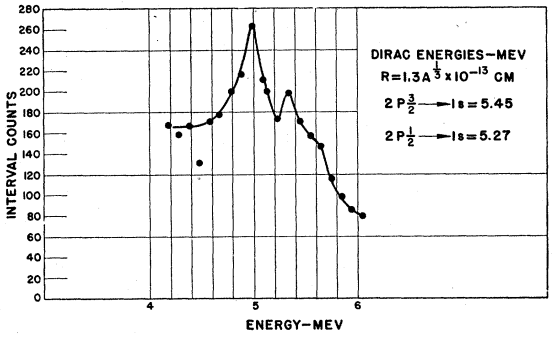

FIG. 16. Pulse-height distribution for Pb with ~100-kev interval width. The main peak at 5.00 Mev is interpreted as the pair production peak due to the x-rays from the $2p_{\frac{3}{2}}\rightarrow 1s$ transition. Further discussion of this curve is in the text. The energy shift due to finite extension is 172 percent of the measured value.

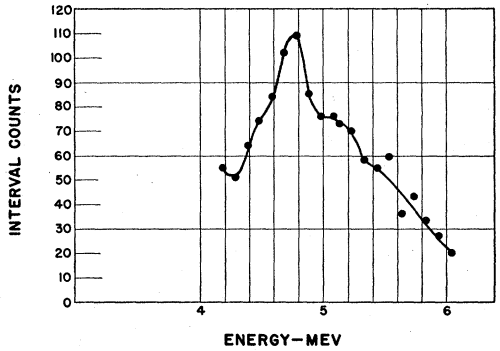

FIG. 17. Pulse-height distribution for Hg($Z=80$). The peak at 4.8 Mev obviously corresponds to the one at 5.0 Mev for Pb.

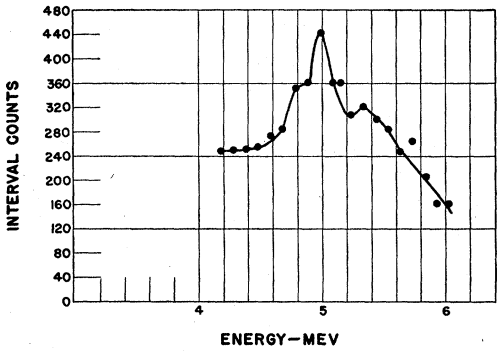

FIG. 18. Pulse-height distribution for Bi($Z=83$). The peak at 5.0 Mev obviously corresponds to the similar peak at the same energy for Pb.

[10] F. Ajzenberg and T. Lauritsen, Revs. Modern Phys. 24, 354–359 (1952).

higher energies are thus the pair and pair plus one annihilation photon peaks for the 6.0-Mev photon. The effects at 4.8 and 5.3 Mev then correspond to the similar peaks for the 5.8-Mev photon. The assymetry and other features would seem to preclude a single photon. The peaks at 5.0 and 5.3 Mev would be hard to reconcile with the expected 0.51-Mev spacing expected for a single photon. Thus we believe that we see the expected fine structure splitting for Pb. The total counts for each point are indicated on the ordinate. The statistics suggest considerable uncertainty in the proper drawing of a curve. However, many separate runs of this type were taken and the essential features of this curve repeated in most of the runs. Thus we believe that the effects are much more likely to be real than the statistics of Fig. 16 alone would suggest. The absence of a large pair peak at 4.0 to 4.7 Mev in Figs. 15 and 16 seems to exclude an interpretation having the x-ray energy near 5.0 or 5.5 Mev. We intend to continue these measurements using a smaller interval width and faster resolving time to eliminate most of the nuclear gamma rays following the absorption of the μ meson.

The similar curves for Hg and Bi are shown in Figs. 17 and 18 and show similar structure. The main peak which came at 5.0 Mev for Pb is at 4.8 Mev for Hg and at 5.0 Mev also for Bi. Rembembering that the x-ray energy increases as the nuclear size decreases, the relatively high energy of the Pb peak compared with that for Bi (i.e., the same x-ray energy for $Z=82$ as for $Z=83$) may be associated with the closed proton shell at $Z=82$, giving a particularly "tight" configuration.

In the analysis of the experimental curves various assumptions are possible about what is assumed "known" or "unknown." Such parameters include (a) the meson mass, (b) the nuclear radius (for a uniform model of the nucleus), (c) the meson spin and magnetic moment. Since the meson mass is known[11] to be close to $210m_e$, we can first consider (b) and (c) using this mass value. As mentioned above, we believe that our results for Pb can best be explained in terms of the expected fine structure splitting for spin $\frac{1}{2}$ and the expected Dirac magnetic moment. Wheeler[8] discusses the expected effect of an anomolous moment.

TABLE IV. Assuming $\mu=210m_e$ and using a uniform nuclear model with $R_0=r_0A^{\frac{1}{3}}$, values of r_0 shown in column 3 gave the best fit to the experimental measured $2p_{\frac{3}{2}}\rightarrow 1s$ transition energies given in column 2 as a function of Z.

Z	$E(2p_{\frac{3}{2}}\rightarrow 1S)$ (experimental, Mev)	r_0 (10^{-13} cm)
22	0.955	1.17
29	1.55	1.21
51	3.50	1.22
82	6.02	1.17

[11] See R. E. Marshak, reference 1, Chap. 6, for a discussion and listing of further reference.

Using $\mu=210m_e$, the nuclear radii which provide the best fit to the data for various elements are given in Table IV. The values all lie near $R_0=1.2\times10^{-13}A^{\frac{1}{3}}$ cm which is much smaller than the radius indicated by other nuclear "size sensitive" experiments. This matter is discussed in more detail below.

For a low-Z element the probability density of the K shell meson near $r=0$ varies as Z^3 and the probability of finding it in the nucleus as $Z^3R_0^3$. The mean change, ΔV, in the potential energy inside the nucleus, because of its nonzero size, is proportional to Z/R_0. Thus the energy shift ΔE due to finite nuclear size should be proportional to $Z^4R_0^2$ for light nuclei. Since the binding energy is proportional to Z^2, the *fractional* energy shift should be proportional to $Z^2R_0^2$. The x-ray energy is relatively insensitive to R_0 for elements of low Z. In the case of Al the total nuclear size effect is only approximately 2 percent. Thus, in principle, the most precise determination of the meson mass could be made using a material of very low Z. However, the limited number of photons producing photoelectrons at the 5819 cathode causes the fractional resolving power of the NaI-5819 detection system to be proportional to $E^{\frac{1}{2}}$ for small E (photon energy). The greatest accuracy in the determination of μ with the present detection system was obtained using $Z=22$, where the energy resolution is not too poor and the nuclear size effect is still small.

The curve for Ti is shown in Fig. 11. Because of the prominent nature of x-ray peak for this element, it was often measured when an over-all check of the operation of the complete system was desired. Since independent calibration runs were made at regular intervals during all runs, a large number of independent evaluations of the x-ray energy for Ti were obtained, all values falling within 1 percent of the mean energy 0.955 Mev. Figure 19 gives a plot of the predicted x-ray energy as abscissa *vs* the μ-meson mass as ordinate. The four lines are for four possible choices of nuclear radius parameter $r_0=R_0A^{-\frac{1}{3}}$ in units of 10^{-13} cm. The experimental results all came within the cross-hatched region about 0.955 Mev. For $\mu=210m_e$, this gives $r_0=1.17\times10^{-13}$ cm in essential agreement with the results for higher Z. The choice $r_0=1.4\times10^{-13}$ cm gives $\mu=217m_e$ which is outside the range allowed by other experimental determinations.

The calculated nuclear radii of a number of elements for $Z=22$ to $Z=83$ (Table IV) are in close agreement and require $r_0\approx1.2\times10^{-13}$ cm, with $r_0=1.17\times10^{-13}$ cm for Pb (in terms of the uniform model). Since many other nuclear-size-sensitive experiments seemed to agree on a choice $r_0=1.4$ to 1.5×10^{-13} cm, and since the precision of the present results for high-Z materials is better than 1 percent for r_0, it is important to examine the present results in more detail. This is done by Cooper and Henley in a following paper.[7] The alternative choices seem to be (a) the present results need large corrections due to effects not considered in the present analysis, or (b) a modification of the "uniform

model" of the nucleus is necessary to account simultaneously for the results of the present experiment and also those of other methods.

Under possibility (a) above we consider the nuclear polarizability in the field of the meson. This would increase the interaction energy and thus the x-ray energy. As mentioned above, estimates[7] of this effect indicate that it is probably less than 0.06 Mev for Pb. The similar results for $Z=80$, 82, and 83 seem to rule out the possibility of any strong "resonance" effect in the polarizability of Pb due to accidental features of the position of its low-lying nuclear energy levels. The second possibility is that there is some additional, at present unknown, specific interaction of μ mesons with nuclear matter. This would have to be an attractive interaction of 3-Mev depth to shift r_0 for Pb from 1.17 to 1.4×10^{-13} cm. Although this possibility cannot be completely dismissed, it seems the least likely of the alternative choices. Thus we believe that neither of these effects are present in significant amount in our measurements.

The alternate choice is to accept the results of the present experiment as stated and also accept the 15 to 20 percent larger results for r_0 of other methods and try to arrive at a nuclear model which will "explain" all of the results simultaneously. To do this we note that total cross sections from scattering experiments, and α-decay lifetimes, are mainly sensitive to conditions at the "edge" of the nucleus. The present experiment is mainly sensitive to the proton density in the inner region of the nucleus and requires an interior charge density $(1.4/1.17)^3=1.7$ times larger (on the uniform model) than do other experiments. This would suggest a nuclear model with a central density two or more times the usually accepted value. The density should then fall off relatively gradually in an extended "edge" region to give the effectively larger radius found by "edge-sensitive" experiments.

It is easily seen that the nuclear "surface" *cannot* be sharp. Even if we consider a nuclear model where the nucleons move in an effective potential with a sharp edge, the nucleon wave functions still have an exponential attenuation in the classically forbidden region. Furthermore, since the effective potential is due to the presence of other nucleons in forming a "self-consistent nuclear box", and in view of the $1\text{–}3\times10^{-13}$ cm range of the basic nuclear forces, the effective potential and nucleon density must require a dropping-off region significantly larger than the range of the nuclear forces.

In α-decay theory, the effective value of R_0 is where the nuclear density is large enough to essentially overcome the Coulomb barrier effects. This is further complicated by the question of the position of the α particle's effective "surface," which must be some distance from its center. The usual addition[12] of 1.2 $\times10^{-13}$ cm for these effects could certainly be much too small.

Similarly, fast neutron scattering experiments are somewhat difficult of exact interpretation for a nucleus with a gradual falling off of nuclear density at the "surface." For neutrons of a few Mev energy particularly, there is probably strong interaction with the outer regions of the nucleus.[13] Similar remarks apply for meson scattering experiments.

The evaluation of nuclear radii for low-Z elements from the Coulomb energy difference of mirror nuclei leads to values of r_0 from 1.39 to 1.47×10^{-13} cm when a uniform model is employed. Since the Coulomb energies for mirror nuclei would seem to have about the same dependence on the nuclear density distribution as does the K-shell μ-meson binding, this would seem to constitute a serious disagreement with the results of the present experiment. However, further study of this matter has been made by Cooper and Henley[7] who find that various corrections should be applied to the mirror nuclei results. Briefly these fall in the following three catagories, all of which tend to reduce the Coulomb energy difference for mirror nuclei.

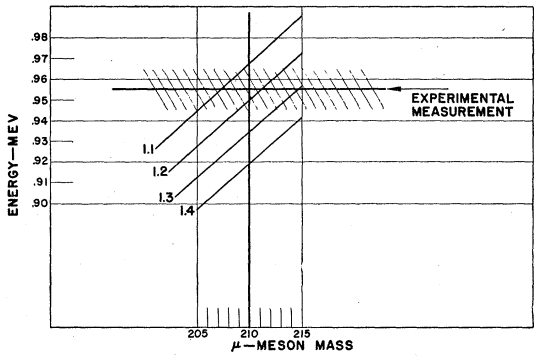

FIG. 19. The $2p\rightarrow1s$ transition energy in Ti as a function of meson mass and nuclear radius. The experimental values all fall within 1 percent of 0.955 Mev. The calculated energies are shown for various values of r_0 in units of 10^{-13} cm, assuming constant proton density inside the nucleus.

The first effect is associated with the Pauli exclusion principle which requires that the total nuclear wave function be antisymmetric in all of the protons. This leads to an excess of space-antisymmetric pairings of protons which means that they have a tendency to correlate their motions in such a way as to *increase* their average spacing. Furthermore, it is not the *average* Coulomb energy per proton that is measured, but the *change* in Coulomb energy when the last nucleon changes from a neutron to a proton. Thus the Coulomb energy difference involves the total increase in the number of antisymmetric pairings when $Z\rightarrow Z+1$. The second effect comes from a study of the predictions of the shell model[14] of Mayer and Haxel, Jensen, and Suess which

[12] See J. M. Blatt and V. W. Weisskopf, *Theoretical Nuclear Physics* (John Wiley and Sons, Inc., New York, 1952), Chap. 11, Eq. (2.19).

[13] R. Jastrow and J. Roberts, Phys. Rev. **85**, 757 (1952).

[14] See P. F. A. Klinkenberg, Revs. Modern Phys. **24**, 63 (1952).

identifies the transforming nucleon as being in a single-particle d state for the important region $Z=9$ to perhaps 20. The radial probability density for a d state gives an effective radius which is appreciably greater than the average over all of the protons, even for a square well potential. If a harmonic oscillator potential is used, the radius at which $E=V$ increases with increasing individual particle energy. Since the transforming nucleon is considered to occupy the highest filled individual-particle state, its wave packet tends to fill a larger volume than the other individual particle wave packets. This third effect is true even for the one-dimensional problem and is thus not directly related to the angular momentum of the state. Considering all of these three effects together, it seems that the mirror nuclei results can probably be brought into agreement with the results of the present experiment. It may be noted that Wilson[15] has reanalyzed the results for mirror nuclei using a gradual falling off of nuclear density at the surface, but without considering the special effects mentioned above.

If a gradual dropping off of nuclear density at the "surface" of the nucleus is assumed, it is still of interest to consider the variation $\rho(r)$ of the proton density inside this boundary region. Feenberg[16] particularly has emphasized the Coulomb repulsion effect and favored a nuclear model where the proton density is larger near the surface than at the center. This leads also to a quite different explanation[16] of the "magic" numbers and is in disagreement with the model more generally favored at present,[14] which essentially assumes a potential closer to that of the oscillator model. In conclusion we note that results for high-energy electron scattering by nuclei were presented by R. Hofstadter *et al.* at the 1953 Washington Meeting of the American Physical Society. Preliminary analysis of their results seemed to favor a model where $\rho(r)$ is a maximum at $r=0$ and drops off steadily at larger r. It seems likely that the most precise determination of the correct $\rho(r)$ *vs* r will come from combining the results of such electron scattering experiments, which suggest the shape of $\rho(r)$ *vs* r, with the μ-meson x-ray results, which give a precision evaluation of the scale factor r_0 for any assumed shape $\rho(r/r_0)$.

It is also possible to obtain information concerning nuclear size by using the results of ordinary (electron) x-ray spectroscopy, as has been pointed out by Schawlow and Townes.[17] The $2p_{\frac{3}{2}}$, $2p_{\frac{1}{2}}$ fine structure splitting for high-Z elements is affected by nuclear size to a very small, but measurable extent. The analysis[17] of available x-ray data gives $r_0 \approx 1.5\times10^{-13}$ cm, with much lower precision than the results of the μ-mesonic x-ray measurements. With improvements in the experimental accuracy of the (ordinary) x-ray measurements, and re-examination of the theoretical analysis to see that no significant higher-order effects (of quantum electrodynamics) have been neglected, the x-ray fine structure splitting should be capable of providing independent, precise information concerning nuclear size.

We wish to thank the many members of the Columbia Physics Department with whom we have discussed various aspects of the problem. Particular thanks are due Dr. Henley and Mr. Cooper, and Professor Wheeler for communication of the results of their calculation prior to publication. Mr. Samuel Koslov has given considerable valuable assistance in the later phases of the experimental measurements and in the calculations.

[15] R. R. Wilson, Phys. Rev. **88**, 350 (1952).

[16] E. Feenberg and K. C. Hammack, Phys. Rev. **75**, 1877 (1949). See also other papers by L. W. Nordheim and M. G. Mayer in the same issue (pp. 1968, 1969, and 1894).

[17] A. L. Schawlow and C. H. Townes, Science **115**, 284 (1952).